

Production and Characterization of Attosecond Bunch Trains

Christopher M.S. Sears,* Eric Colby, Rasmus Ischebeck, Christopher McGuinness,
Janice Nelson, Robert Noble, Robert H. Siemann, James Spencer, and Dieter Walz

Stanford Linear Accelerator Center, Menlo Park CA 94025

Tomas Plettner and Robert L. Byer

Stanford University, Stanford CA 94305, USA

(Dated: February 1, 2008)

Abstract

We report the production of optically spaced attosecond microbunches produced by the inverse Free Electron Laser (IFEL) process. The IFEL is driven by a Ti:sapphire laser synchronized with the electron beam. The IFEL is followed by a magnetic chicane that converts the energy modulation into the longitudinal microbunch structure. The microbunch train is characterized by observing Coherent Optical Transition Radiation (COTR) at multiple harmonics of the bunching. The experimental results are compared with 1D analytic theory showing good agreement. Estimates of the bunching factors are given and correspond to a microbunch length of 350as fwhm. The formation of stable attosecond electron pulse trains marks an important step towards direct laser acceleration.

PACS numbers: 41.75 Jv, 41.60 Cr, 41.60.Dk, 41.85.Ct

Submitted to Physical Review Letters

The continued development of short pulse, high peak intensity lasers has led to great interest in their application to particle acceleration. Recently, such lasers have succeeded in producing semi-monoenergetic beams from plasma wakefield interactions[1–3]. These experiments relied on very large terawatt class systems and accelerated indirectly by inducing a “bubble”-shaped wake in a plasma and accelerating a beam of trapped plasma electrons. Lasers have also been used for direct acceleration between laser and beam via IFEL interactions [4, 5], Inverse Cherenkov acceleration [6], and Inverse Transition Radiation [7]. These experiments also relied on high power, low repetition rate lasers for acceleration. The transverse dimensions were much larger than the accelerating wavelength, leading to low coupling efficiency[8]. An altogether different approach to laser acceleration we are pursuing confines the beam and laser in an optical scale accelerating structure. While the peak electric fields will still allow for a considerable accelerating gradient, approaching 1 GeV/m, the small dimensions mean the total power needed will be very low, just $\mu\text{J}/\text{pulse}$, which can be provided at high repetition rate by a mode locked oscillator.

To one day take advantage of high repetition rate laser sources requires wavelengths in the optical to near-infrared. This wavelength region also has the most active research in near-field structures such as photonic bandgap fibers[9] and lithographic optical components. To investigate near-field infrared laser acceleration an IFEL microbuncher has been designed and tested at 800nm. IFEL production and acceleration of microbunches has been demonstrated at $10.6\text{ }\mu\text{m}$ [4]. At the shorter wavelength needed for this research program tolerances are an order of magnitude tighter. This research therefore marks an important first step in developing near-field IR laser accelerators.

The microbuncher used in this experiment comprises a magnetic undulator in which the beam energy is modulated by an IFEL interaction and a chicane that converts the energy modulation into a density modulation through the chicane R_{56} . The IFEL alone has been demonstrated previously in an experiment exploring various harmonics of the IFEL interaction[10]. The IFEL interaction plus chicane produces a train of few hundred attosecond pulses spaced at the laser period (2.3 fs). Although microbunched beams have been well-studied from FELs, producing them via an IFEL has the considerable added experimental difficulty of aligning the pre-existing laser beam to the electrons. However, using an IFEL allows optical phase control of the microbunches, a requirement for net acceleration in a two-stage experiment, and substantially reduces the length of the undulator

required to form bunches.

To verify the existence of the microbunches the beam is sent through a foil to produce COTR. As with velocity bunched klystron beams[11], the microbuncher forms a density modulation with strong harmonic content. This density modulation can be expressed as a Fourier series whose coefficients are Bessel functions depending on the amount of dispersion (R_{56}) imparted and the modulation from the IFEL[12, 13]. The intensity of COTR at each harmonic is then proportional to the square of the density modulation giving equation (1) where η is the amplitude of the sinusoidal IFEL modulation normalized to the beam energy, σ_γ is the fractional initial energy spread, k_L is the laser wavenumber, and n is the harmonic number [14].

$$I_{COTR} \propto [J_n(nk_L R_{56}\eta)]^2 \exp \left[- \left(\frac{n\eta}{\sigma_\gamma} \right)^2 \right] \quad (1)$$

The R_{56} of the chicane is found by integrating the Lorentz equations and is given in equation (2) where L is the distance from the undulator to the COTR radiator and B_y is the chicane magnetic field. The first term in the expression comes from velocity bunching which gives a small but non-negligible contribution to the total R_{56} .

$$R_{56} = \frac{L}{\gamma^2} + \left(\frac{q}{\gamma m_e c} \right)^2 \int_0^L \left[\int_{-\infty}^z B_y(z') dz' \right]^2 dz \quad (2)$$

Direct comparison of the experimental results to the analytic theory is complicated by several issues, most appreciably the non-uniformity of the laser field transversely and in time. In the real experiment there is not a constant modulation η for every electron in the bunch. As a result, certain portions of the beam will optimally bunch at different values of R_{56} and will similarly radiate most strongly at different values.

This research was conducted at the NLCTA facility at SLAC, a 60 MeV Xband accelerator that was recently upgraded with an Sband photoinjector for laser acceleration research. The NLCTA beamline includes a chicane for energy collimation. Using the energy collimation, the accelerator produces 1pC, $\sim 1ps$ pulses with $\leq 0.05\%$ energy spread. The laser system used to produce UV for the photoinjector also provides IR pulses for laser acceleration research. This setup gives the timing stability necessary for experiments[15].

The beam enters a separate experimental hall via a 25° dogleg bend. The laser for the IFEL is introduced at an optical window at the second dogleg bend. Both beams are focused

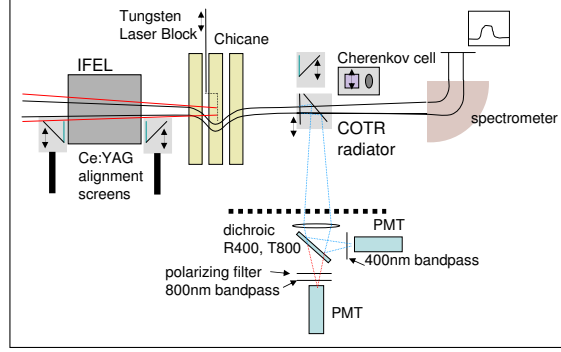


FIG. 1: Layout of the microbunching experiment.

going into the experimental chamber housing the undulator, chicane, and the COTR radiator as well as several diagnostic screens (see figure 1). Two Ce:YAG screens are attached fore and aft of the undulator for overlapping the laser and electron beam while a third screen is used to minimize the electron beam spot size at the radiator. A Cherenkov radiator is also located in the experimental chamber for obtaining picosecond-class timing of the laser to electron beam using a streak camera. After the experimental chamber the beam enters a 90° imaging energy spectrometer with 5 keV resolution. The COTR radiator is located at the image point of the energy spectrometer coinciding with the minimum electron spot size. This gives optimal resolution at the spectrometer and prevents the induced scatter from the foil from effecting the measured energy spectrum.

To avoid damaging the COTR radiator and to reduce background due to the laser, a tungsten beam stop is inserted in the middle of the chicane to intercept the laser after it is used for the IFEL. The radiator consists of two pellicle mirrors, one normal to the beam and a second at 45° to send the light to a pair of photomultiplier tubes (PMTs). The COTR light is split using a dichroic mirror to reflect the second harmonic to one PMT and transmit the fundamental to the second. Each PMT also has a bandpass filter attached to select only the given harmonic and also help protect against ambient light. Finally, a polarizing filter is placed in front of the 800nm PMT to further reduce background due to the laser.

Table (I) gives a list of experimental parameters including beam, laser, and magnet values. The beam values for the initial energy spread and temporal pulse length were obtained from the data itself. Data are taken in runs of 500-4000 beam shots at 10 Hz. A fast delay mirror is used to vary the delay between the electron beam and laser before each shot. For each

Parameter	Value
Electron Energy	60 MeV
Energy Spread	30 keV (typ.)
Electron Pulse length	0.8ps* (typ.)
Electron Spot Size	100 μm (nom.)
Bunch Charge	1pC (nom)
Laser Wavelength	785 nm
Laser Energy	0.65 mJ/pls
Laser Pulse length	0.5ps (nom.)
Laser Spot Size	200 μm
Undulator Period	1.8 cm
Number of Periods	3
Undulator Strength (a_w)	0.46
Chicane R_{56}	0.04-0.16 mm

TABLE I: Experimental Parameters for attosecond bunch train production. All widths are given as fwhm. *Estimated from the data.

shot an image of the beam at the energy spectrometer is acquired along with numerous diagnostics including the COTR PMTs and diodes for the laser. From the energy profiles a beam energy spread is extracted and plotted against the delay forming a cross-correlation scatter plot. When the electron beam and laser are in time the IFEL modulates the electron beam energy and the COTR signal is strongest.

The cross-correlation is an important technique for this experiment, especially for the COTR signal. The fact that the signals from the PMTs are strongest when the laser and electron beam are in-time excludes other processes as background including harmonic generation from the laser hitting surfaces in the chamber, incoherent transition radiation, bremsstrahlung, or undulator radiation, all of which would occur regardless of relative timing between the two beams.

Figure (2) shows an example data run showing the cross-correlation scatter plots of the energy spread as well as the fundamental and second harmonic COTR signals. In this

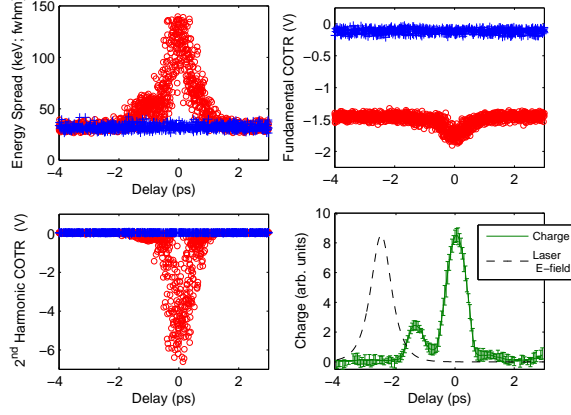


FIG. 2: Example data run of the IFEL microbunching experiment containing 2130 events. Top left is the electron energy spread as a function of delay with laser-on events in red (circles), laser-off in blue (crosses). Also shown are the COTR raw signals at the fundamental (top right) and second harmonic (bottom left). The bottom right figure shows the current profile calculated by deconvolving the laser pulse from the cross-correlation data.

particular beam configuration there is a smaller electron pulse behind the main pulse. Deconvolution of the laser temporal profile from the modulation (fig. 2 bottom right) estimates the main electron pulse temporal length of 0.8ps fwhm. The COTR signals show the same characteristic structure to the beam. The fundamental COTR signal has a large offset between laser-on and laser-off events indicating there is still significant bleed-through of laser light to the detector. This bleed-through also contributes significantly to the noise on the signal.

To explore further the dependence of COTR output on the IFEL modulation we plot the COTR signals versus the IFEL modulation strength. This is shown in figure (3). Here, the raw COTR signals have been inverted, rescaled, and the baseline signal (with no IFEL interaction) subtracted. The IFEL modulation is given by the difference in quadrature of the total energy spread and the initial energy spread ($\sigma_{IFEL} = \sqrt{\sigma_{TOT}^2 - \sigma_{init}^2}$). The only cut applied to the data here is on the delay timing to select events near the interaction overlap.

Shown with the data for each harmonic is the analytic form (eqn (1)) using the known value of $R_{56} = 0.2mm$ and taking $\eta = 0.5 * M * 1.3$ where M is the measured IFEL modulation fwhm. For a constant modulation across the entire beam, we would have $\eta = 0.5 * M$ (recall η is the amplitude of a sinusoidal modulation). However, since the measured M is an

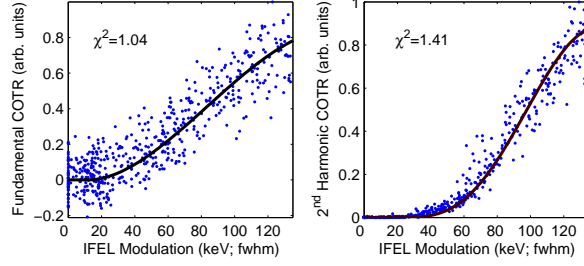


FIG. 3: Scatter plot of COTR signals versus IFEL modulation for a single run. Each point is a single interaction of the laser and electron beam. The amplitude of the IFEL interaction varies due to the delay scan. The solid lines give the analytic form (eqn. (1)).

average across the entire beam including electrons not modulated (either out-of-time or off-axis transversely), we expect the radiating portion of the beam to have a larger modulation η . Allowing η as a fit parameter and minimizing χ^2 we obtain $\eta = 0.65 * M$. This is also consistent with an extended analytic theory taking into account laser and electron beam form factors. The fit of the analytic form to the data shows very good agreement with $\chi^2 = 1.06$ for the fundamental data and $\chi^2 = 1.4$ for the second harmonic. For this fit the variance for each data point is calculated from the deviation of the nearest neighbors.

With the COTR signals plotted in this way the difference in the two harmonics is clear. As the total IFEL modulation decreases the amount of second harmonic COTR falls off more rapidly than the fundamental. This is due both to the differing Bessel function dependence as well as to the greater sensitivity to energy-spread-based washout from the exponential term in equation (1).

In addition to the modulation strength, η , the COTR output varies strongly with the chicane R_{56} . The chicane design includes coils to give adjustment of the magnetic field by up to $\pm 20\%$ in order to optimize microbunch formation. To study the dependence of COTR output versus chicane strength, a number of short data runs were taken with the chicane strength varied between each run. A fit was done to each cross-correlation, an amplitude extracted and an error deduced using boot-strap method. The results are shown in figure (4).

The main difference between the two curves in the chicane scan comes at low values of R_{56} where the second harmonic again rolls off faster than the fundamental. At higher values both signals show a roll-off indicating that optimum bunching is being reached for

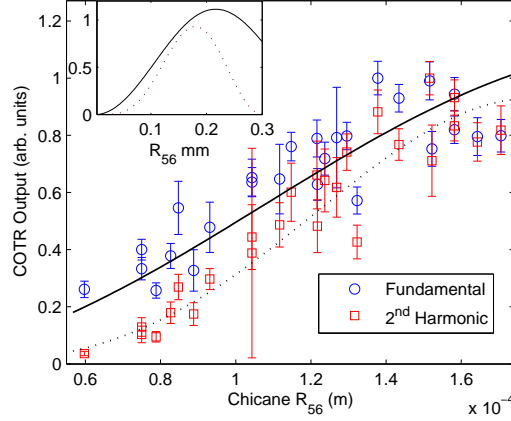


FIG. 4: A scan of the chicane R_{56} . The first and second harmonics are shown together with the analytic form overlayed. Each data point represents a run of 500 events, fitted with errors found by the boot-strap technique. The inset shows the analytic function for the COTR output (equn. (1)).

$R_{56} = 0.13 - 0.16\text{mm}$. The inset shows the analytic form over a larger range of R_{56} taking $\eta = 0.65 * M$ as before where for these runs the mean interaction $M = 100\text{ keV fwhm}$. These runs were taken over a period of ~ 1 hour during which both the mean interaction strength M and the total charge drifted. As a result, the fit to the analytic form is relatively poor compared to the COTR versus modulation data shown in figure (3). Nevertheless, the data agrees well qualitatively with the analytic form. The analytic solutions reach a maximum at $R_{56} = 0.22\text{mm}$ for the fundamental and 0.18mm for the second harmonic. The actual COTR signals peak for lower R_{56} due to the mean being pulled down by more strongly interacting events that are overbunched. Figure 2 shows events with modulation up to 140keV . For these events, optimal bunching would occur at $R_{56} = 0.12\text{mm}$. This demonstrates the importance of independently measuring the bunching through the COTR to optimize the R_{56} .

A number often quoted as a figure of merit for bunching is the bunch parameter b_n , equal to the Fourier coefficient for longitudinal charge density. In our case: $b_n = J_n(nR_{56}k_L\eta)\exp[-\frac{1}{2}(n\sigma_\gamma/\eta)^2]$. For the maximum R_{56} strength and the modulation $M = 100\text{keV}$ we obtain $b_1 = .52$ and $b_2 = 0.39$. At this level of bunching the individual microbunches have a temporal pulse width of $\sim 350\text{as}$.

This experiment has succeeded in producing stable, optically spaced attosecond bunch trains. With the laser to electron beam delay held constant, a microbunched beam is pro-

duced on every shot with a jitter corresponding to $\leq 20\%$ on the bunching factor. This stability will be important in future experiments looking to measure net acceleration of optical microbunches in near-field structures. Prior to powered acceleration experiments, the microbunched beam will also help probe candidate accelerators structures by studying the wakes produced by the passage of a microbunched beam through a near-field optical structure. This research effort will lead to novel devices producing energetic beams at very high repetition rates.

The authors wish to acknowledge the efforts and contributions of the NLCTA Operations group: Justin May, Doug McCormick, Tonee Smith, Richard Swent, and Keith Jobe. We would also like to thank Walt Zacherl and Bruce Rohrbough for their work on laser diagnostics. This work is supported by Department of Energy contracts DE-AC02-76SF00515 and DE-FG02-03ER41276.

* `cmsears@slac.stanford.edu`

- [1] J. Faure, Y. Glinec, A. Pukhov, S. Kiselev, S. Gordienko, E. Lefebvre, J. Rousseau, F. Bourgy, and V. Malka, *Nature* **431**, 541 (2004).
- [2] S. M. et al., *Nature* **431**, 535 (2004).
- [3] C. Geddes, C. Toth, J. van Tilborg, E. Esarey, C. Schroeder, D. Bruhwiler, C. Nieter, J. C. J, and W. Leemans, *Nature* **431**, 538 (2004).
- [4] W. Kimura, A. van Steenbergen, M. Babzien, L. C. I. Ben-Zvi, D. Cline, C. Dilley, J. Gallardo, S. Cottschalk, and P. H. et al., *Physical Review Letters* **86**, 4041 (2001).
- [5] P. M. et al., *Physical Review Letters* **94**, 154801/1 (2005).
- [6] W. K. et al., *Physical Review Letters* **74**, 546 (1995).
- [7] T. Plettner, R. L. Byer, E. Colby, B. Cowan, C. M. S. Sears, J. E. Spencer, and R. H. Siemann, *Physical Review Letters* **95**, 134801 (pages 4) (2005).
- [8] Y. C. N. Na, R. H. Siemann, and R. L. Byer, *Phys. Rev. ST Accel. Beams* **8**, 031301 (2005).
- [9] B. Cowan, *Physical Review Special Topics: Accelerators and Beams* **6** (2003).
- [10] C. M. S. Sears, E. R. Colby, B. M. Cowan, R. H. Siemann, J. E. Spencer, R. L. Byer, and T. Plettner, *Physical Review Letters* **95**, 194801 (pages 4) (2005).
- [11] P. Webster, *J. Appl. Phys.* **10**, 501 (1939).

- [12] S. Baccaro, F. D. martini, and A. Ghigo., Opt. Lett. **7**, 174 (1982).
- [13] A. Luccio, G. Matone, L. Miceli, and G. Giordano, Laser and Particle Beams **8**, 383 (1990).
- [14] Y. Shibata, T. Takahashi, T. Kanai, K. Ishi, M. Ikezawa, J. Ohkuma, S. Okuda, and T. Okada, Phys. Rev. E **50**, 1479 (1994).
- [15] C. M. et al., Proceedings of PAC 2007, Albuquerque, New Mexico, USA (2007).